Soft Matter

Accepted Manuscript

This is an *Accepted Manuscript*, which has been through the Royal Society of Chemistry peer review process and has been accepted for publication.

Accepted Manuscripts are published online shortly after acceptance, before technical editing, formatting and proof reading. Using this free service, authors can make their results available to the community, in citable form, before we publish the edited article. We will replace this *Accepted Manuscript* with the edited and formatted *Advance Article* as soon as it is available.

You can find more information about *Accepted Manuscripts* in the Information for Authors.

Please note that technical editing may introduce minor changes to the text and/or graphics, which may alter content. The journal's standard Terms & Conditions and the Ethical guidelines still apply. In no event shall the Royal Society of Chemistry be held responsible for any errors or omissions in this *Accepted Manuscript* or any consequences arising from the use of any information it contains.

ROYAL SOCIETY OF CHEMISTRY

www.rsc.org/softmatter

Journal Name

ARTICLE TYPE

Cite this: DOI: 10.1039/xxxxxxxxxx

Interfacial rheometry of polymer at a water-oil interface by intra-pair magnetophoresis†

Stefano Cappelli,[ab] Arthur M. de Jong,[ab] Jean Baudry,[c] and Menno W.J. Prins[abd]

Received Date
Accepted Date

DOI: 10.1039/xxxxxxxxxx

www.rsc.org/journalname

We describe an interfacial rheometry technique based on pairs of micrometer-sized magnetic particles at a fluid-fluid interface. The particles are repeatedly attracted and repelled by well-controlled magnetic dipole-dipole forces, so-called interfacial rheometry by Intra-Pair Magnetophoresis (IPM). From the forces (∼pN), displacements (∼ μm) and velocities (∼ μm/s) of the particles we are able to quantify the interfacial drag coefficient of particles within a few seconds and over very long timescales. The use of local dipole-dipole forces makes the system insensitive to fluid flow and suited for simultaneously recording many particles in parallel over a long period of time. We apply IPM to study the time-dependent adsorption of an oil-soluble amino-modified silicone polymer at a water-oil interface using carboxylated magnetic particles. At low polymer concentration the carboxylated particles remain on the water side of the water-oil interface, while at high polymer concentrations the particles transit into the oil phase. Both conditions show a drag coefficient that does not depend on time. However, at intermediate polymer concentrations data show an increase of the interfacial drag coefficient as a function of time, with an increase over more than three orders of magnitude (10^{-7} to 10^{-4} Ns/m), pointing to a strong polymer-polymer interaction at the interface. The time-dependence of the interfacial drag appears to be highly sensitive to the polymer concentration and to the ionic strength of the aqueous phase. We foresee that IPM will be a very convenient technique to study fluid-fluid interfaces for a broad range of materials systems.

1 Introduction

Macromolecules, such as proteins, surfactants and nanoparticles, are known to strongly bind to and thereby modify fluid-fluid interfaces, with applications in food processing technologies for the stabilization of foams and emulsions,[1,2] micro-encapsulation techniques for personal care[3] and drug delivery,[4,5] and in the creation of new functional materials based on self-assembly.[6,7] Upon adsorption, the interface becomes crowded and the interaction between the adsorbed species strongly changes the mechanical properties of the fluid-fluid interface.[2,8–15] Studies of these processes require rheometry techniques that are suited for small amounts of materials, small length scales, short and long timescales, and that are easy to use. Conventional interfacial rheometers have a limited sensitivity due to the size of the probes typically millimeter or larger, and are not suited for biomedical research, where the amounts of material are generally limited and the relevant scales are well below the millimeter scale.[16–19]

Microrheology refers to the use of micrometer-sized objects to measure interfacial shear viscosities on small length scales (∼ μm), small sample volumes (∼ μL), and with a high sensitivity.[11,15,16,18–21] The sensitivity to the interfacial viscosity is expressed through the Boussinesq number *Bo*, which for a water-oil interface and a probe of characteristic dimension a can be expressed as:

$$Bo = \frac{\eta_S}{a(\eta_{water} + \eta_{oil})} \quad (1)$$

where η_S is the interfacial viscosity, η_{water} and η_{oil} are the bulk viscosities of water and oil respectively. If $Bo >> 1$ the motion of the probe is decoupled from the hydrodynamics of the subphases and is dominated by the interfacial shear viscosity η_S. Microrheology can be divided in passive[17,19,20,22] and active methods.[23–28] In passive microrheology the Brownian motion of a probe is followed in time and is related to its diffusivity using a mean-squared displacement (MSD) analysis.[11] The accuracy of

[a] Department of Applied Physics, Eindhoven University of Technology, Eindhoven, The Netherlands.
[b] Institute for Complex Molecular Systems (ICMS), Eindhoven University of Technology, Eindhoven, The Netherlands.
[c] Laboratoire Colloïdes et Matériaux Divisés, Institute of Chemistry, Biology and Innovation ESPCI ParisTech/CNRS UMR 8231/PSL* Research University, Paris, France.
[d] Department of Biomedical Engineering, Eindhoven University of Technology, Eindhoven, The Netherlands. E-mail: m.w.j.prins@tue.nl

† Electronic Supplementary Information (ESI) available. See DOI: 10.1039/b000000x/

Soft Matter Accepted Manuscript

this method relies on the correct estimation of the drift (due to thermal convection, Marangoni effect, sample, etc.) that is superimposed on the thermally activated motion of particles. The drift can be corrected by subtracting the average motion of an ensemble of trajectories or by following the motion of a fixed reference object. For high viscosities ($\eta_S > 10^{-6}$ Ns/m) the static noise of the setup is generally comparable to the particle average displacement, and an incorrect estimation of the drift leads to systematically lower values for interfacial viscosities.[19] Two-particle microrheology overcomes these limitations by extracting the particle diffusivity from ensemble-averaged cross-correlated motion and inter-particle distances, which however requires a large amount of trajectories to be recorded.[29]

In active microrheology external forces control the motion of the probes, such as generated with optical or magnetic tweezers. These forces allow one to reduce the number of probes required, to measure interfacial viscosities as high as $\eta_S \sim 10^{-4}$ Ns/m, and to reduce the measurement time to a few seconds, ideal to study time dependent phenomena. Optical tweezers have mainly being used to study the rheology of bulk fluids[30–34] and in some cases also for fluid-fluid interfaces.[35–37] The position of the probe is controlled with nanometer accuracy and it is possible to apply a wide range of forces. Magnetic tweezers have the advantage of low interference, because organic materials are fully permeable and insensitive to magnetic fields. With the use of micro-fabricated probes, such as magnetic nanowires and magnetic micro-buttons, magnetic tweezers have been successfully used to study the ageing of protein films[23,26,27] and the shear viscosity of phospholipid and surfactant monolayers.[25,28] The forced motion of a probe allows one to bring the system out of equilibrium and to explore many interesting and important material properties. However, the geometry of the probe and the dynamics of the actuation play an important role, as different rheological deformations such as dilatational and shear contributions might be coupled in one experiment. This makes the interpretation of data dependent on the material system under study, the conditions of the experiment and on assumptions of the hydrodynamic model used.[19,38–40]

In this paper we describe an interfacial rheometry technique based on pairs of micrometer-sized magnetic particles that are repeatedly attracted and repelled by well-controlled magnetic dipole-dipole forces, so-called interfacial rheometry by Intra-Pair Magnetophoresis (IPM)[41] (Fig. 1a,b). From the forces, displacements and velocities of the particles one can quantify the interfacial drag coefficient within a few seconds and over very long timescales. This approach does not require microfabricated probes and operates with commercially available magnetic particles, which are nowadays available with a wide range of sizes, material and optical properties, and which can be easily functionalized to suit a wide range of applications.[42] The use of local dipole-dipole forces makes the method insensitive to fluid flow and suited for parallelization. Moreover, this method allows one to study proximity effects during particle separation and approach under different forces and shear rates.

We first validate the use of IPM for the measurement of viscous drag coefficients by comparing IPM data of particles in bulk water to data of Brownian motion analysis. Then, we study the dependence of interfacial drag on the adsorption of an amino-modified silicone polymer to a water-oil interface (Fig. 1c). Polyelectrolytes have a broad range of applications, such as for the production of microcapsules for biomedical applications,[43] food science,[44] and personal care products.[3] In these systems, the time-dependent adsorption of polyelectrolytes to water-oil interfaces plays an important role in the production method and determines the final material properties.[5] At low polymer concentration the IPM particles remain mainly in the water side of the water-oil interface, while for high concentrations the particles transit into the oil phase (Fig. 1d). In both cases measurements show values of drag coefficients independent of time. However at intermediate polymer concentrations the data show an increase of the interfacial drag coefficient by several orders of magnitude as a function of time and of fluid composition.

2 Materials and methods

2.1 Materials

We use a silicone-based polymer functionalized with diamino-groups on the side chain (KF8004, provided as samples by Shin-Etsu Silicones Europe B.V.). The polymer is soluble only in the oil phase and concentrations are prepared by weighting the components. The radius of gyration of the polymer in oil was measured using dynamic light scattering (DLS), which results in $R_G = 15 - 20$ nm. The oil phase is isononyl-isononanoate (Lanol 99, Seppic, $\eta_{oil} = 6$ mPa·s). The aqueous phase consists of phosphate buffered saline (PBS), prepared by dissolving PBS tablets (PBS tablets, pH 7.4, Sigma Aldrich) in 200 mL of ultra-pure water (resistivity > 18.2 MΩ·cm) according to the supplier and then further diluted. All the components were used as received from the suppliers, without any further purification step.

We use carboxylic superparamagnetic particles (Dynabeads M-270 carboxylic acid, diameter $2R = (2.8 \pm 0.1)$ μm, Life Technologies) as probes in all the experiments. In the presence of a magnetic field, the induced magnetization follows a Langevin function, with a particle-to-particle variation of magnetic susceptibility of about 8%.[41] Particles were magnetically washed four times in ultra-pure water in order to remove surface-active elements present in the storage buffer, and were then dispersed in each corresponding buffer in a ratio 1 : 10000 from the stock solution.

Soft Matter Accepted Manuscript

This journal is © The Royal Society of Chemistry [year]

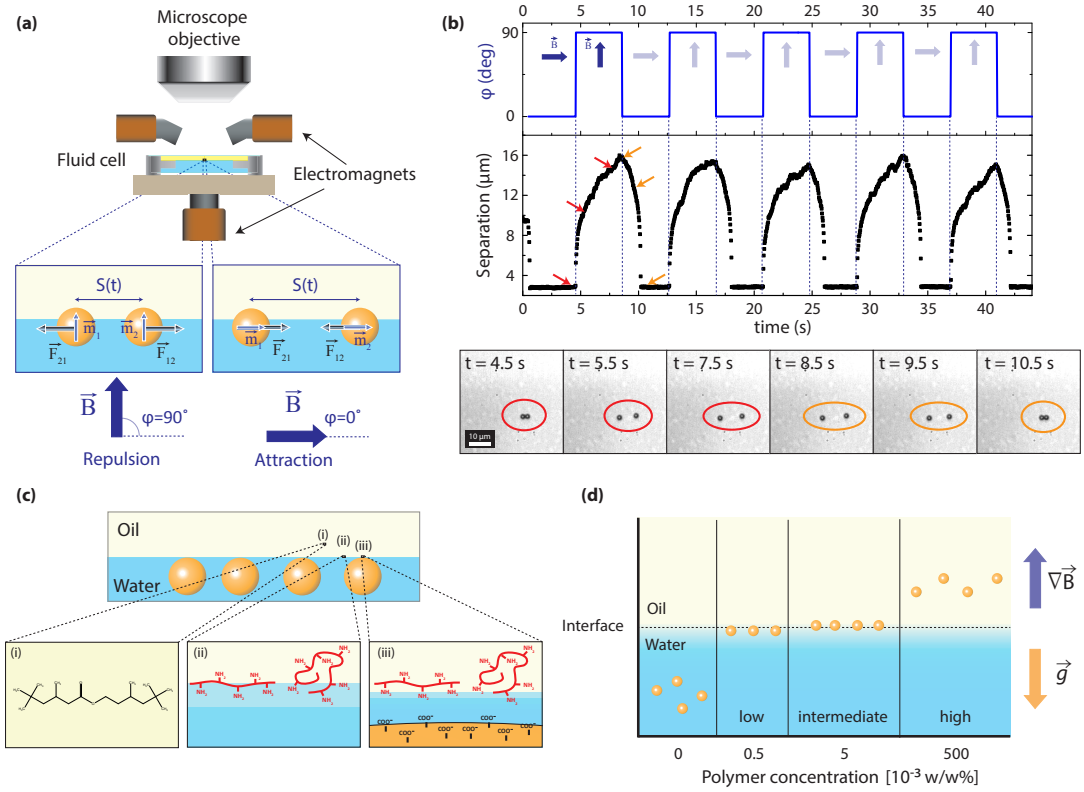

Fig. 1 Principle of the Intra-Pair Magnetophoresis (IPM) experiment. (a) Pairs of particles are repelled and attracted by changing the orientation of the magnetic field φ generated by a set of electromagnets. Trajectories are recoded using a digital camera mounted on an optical microscope. (b) A typical IPM experiment consists of five repulsions and attractions. Center-to-center separation distance curves are extracted from the digital images (bottom). The drag is calculated by fitting the average of five repulsions to eqn (3). (c) Magnetic particles at a water-oil interface: oil-soluble amino-modified silicone polymer is dispersed in the oil phase (i) and adsorbs to the interface (ii). At the fluid-fluid interface, carboxylated magnetic particles (with negative charge) interact electrostatically with the amino-modified polymer (with positive charge) (iii). (d) Position of the particles as a function of polymer concentration c_P. Particles are brought into contact with the interface by means of magnetic field gradients. The particles sediment to the bottom of the fluid cell by gravitational forces when no polymer is present in the oil phase. The particles adsorb and retain a position in the interface when polymer is present at a low or intermediate concentration. The particles transit into the oil phase when polymer is present at a high concentration.

Soft Matter Accepted Manuscript

2.2 Positioning of the particles at the interface

We create a flat water-oil interface using a custom made fluid cell (ESI†, Fig. S1) which consists of two circular aluminum rings. The outer ring, with a bottom hole to host a glass coverslide (19 mm diameter, Thermo Scientific™), contains the inner ring with a central hole with sharp edges where the water phase pins. The oil phase is gently deposited on top of the water phase and the cell is closed with a glass coverslide (24 mm diameter, Thermo Scientific™). The moment when the oil-water interface is formed sets the starting point for the reference time (adsorption time t_A) in our experiments. The whole system is held by capillary forces and we found the interface to be stable for several hours. Prior to any measurements all the fluid cell components (inner rings and glass cover slides) were washed in a sonic bath for 10 min first in acetone and then in isopropanol, ethanol (Sigma Aldrich), and finally in ultra-pure water.

After assembling the fluid cell, we bring the particles from the water phase to the interface by shortly applying a vertical magnetic force with a permanent magnet. After removing the magnet, the particles that are not trapped at the interface sediment to the bottom of the fluid cell. The microscope (Leica, DM6000 B) is equipped with a motorized stage that allows us to locate the position of the focal plane with micro-meter accuracy, thereby the position of the particles within the fluid cell. The concentration of particles is chosen in order to have a low surface coverage at the interface (< 0.1 %) so as to limit particle-particle interactions.

2.3 Particle tracking

We visualize the probes with a 40x magnification (0.40 N.A.) and acquire images with a high speed CMOS camera (MotionPro X3, Redlake) with a sampling rate of 30 frames per second. The trajectories of the particles are reconstructed from digital image analysis of consecutive frames with in-house written Matlab routines. Briefly, images (Fig. 1b bottom) are filtered with a low-pass Gaussian filter and corrected for the background. The particle center is determined using an algorithm based on the Hough transform, which looks for a set of pixels belonging to the same geometrical object, in our case a circle.[45] Other computationally more efficient strategies, such as cross-correlation or centroid tracking, cannot be used in this study as they fail to track objects that are in close proximity. Finally, the particle positions are correlated through consecutive frames using a Matlab implementation of the algorithm developed by Crocker and coworkers.[46,47]

2.4 Interfacial rheometry by Intra-Pair Magnetophoresis (IPM)

Intra-Pair Magnetophoresis (IPM) was previously developed in our group to quantify distributions of the magnetic properties of superparamagnetic particles.[41] Here, we expand the use of IPM for rheometry studies of particles at fluid-fluid interfaces. We actuate magnetic particles by positioning the sample between a set of five electromagnets with soft iron cores, four of which are positioned above (normal to each other) and one below the sample (Fig. 1a). The intensity and the direction of currents in the electromagnets (e.g. the magnetic fields) are controlled with a LabView interface that allows us to program any arbitrary actuation sequences (e.g. Fig. 1b). With this geometry we can apply magnetic fields with a magnitude between 0.1 and 50 mT.

When a superparamagnetic particle is exposed to a magnetic field it acquires a magnetic moment along the direction of the field, and a magnitude that scales with the field intensity, following approximately a Langevin function.[41] When two particles are in close proximity we can exploit their magnetic dipole-dipole interaction in order to induce magnetic attraction or repulsion (insets Fig. 1a). If we apply a field normal to the plane of the interface (out-of-plane), the force is repulsive and the center-to-center separation distance S increases. The motion of the particles is opposed by the hydrodynamic drag. In a material system with linear dependence of drag force on velocity, the following equations apply:

$$F_{dd} = \frac{3\mu_0 m_1 m_2}{4\pi S^4}, \qquad F_{drag} = \frac{f}{2} \cdot \frac{dS}{dt} \tag{2}$$

where F_{dd} is the dipole-dipole induced magnetic repulsive force, μ_0 is the vacuum permeability, m_i is the magnitude of the induced magnetic moment (in units Am^2) for particle i, F_{drag} is the drag force and f is the hydrodynamic drag coefficient (in units Ns/m). Inertia can be neglected, since the Reynolds number (ratio between inertial and viscous forces) for the system under study is $Re \approx 10^{-6} << 1$.

The forces in eqn (2) define the equation of motion, and the solution of the differential equation yields

$$S(t)^5 = \frac{15\mu_0}{2\pi} \cdot \frac{m_1 m_2}{f} \cdot t + S_0^5 \tag{3}$$

where S_0 is the separation distance at time $t_0 = 0$. The repulsive magnetic force is always aligned with the inter-particle distance vector and does not depend on the orientation of the pair. If the magnetic field is now applied parallel to the interface (in-plane field, Fig. 1a) the resulting magnetic dipole-dipole force is attractive, with a solution that is of the same form as eqn (3) but has a different prefactor. This force depends on the relative orientation between the applied magnetic field and the inter-particle distance vector, but with the actuation protocol used in our experiments, the pair orientation hardly deviates from the field orientation (Fig. 1b, section S2, ESI†). Details of the calculations can be found in reference [41].

A typical IPM experiment is shown in Fig. 1b. Particles are repeatedly attracted and repelled by changing the orientation of

Soft Matter Accepted Manuscript

This journal is © The Royal Society of Chemistry [year]

the magnetic field every 5 seconds, and images are acquired at a rate of 30 frames per second. The intra-pair separation distance S is extracted from digital image analysis (see previous section) and the drag coefficient is obtained by fitting the average of 5 curves with eqn (3). The drag coefficient is obtained by assuming a linear relationship between drag force and translational particle velocity, i.e. a Newtonian system. However, soft-matter systems can also exhibit non-linear properties. For example, polymer solutions can be viscoelastic, with a drag force that depends on the velocity history.[48,49] The hydrodynamic properties of fluid-fluid interfaces may also depend on the type of adsorbed species.[18,23] For the material system in this paper, we find that the response is essentially linear, so that the motion of the particles is dominated by the linear shear response of the interface.

2.5 Interfacial rheometry by Mean-Squared Displacement (MSD)

The viscous drag of a fluid can be determined by the thermally activated motion of particle probes, i.e. Brownian motion.[11] From the trajectory of particles it is possible to calculate the diffusion coefficient D from the mean-squared displacement according to

$$< (r(t+\tau) - r(t))^2 >= 2dD \cdot \tau \quad (4)$$

where $r(t)$ is the position of the particle at time t, τ is the lag time, d is the dimensionality of the system, and D is the diffusion coefficient of the particles. In our experiments the average is performed over all the particles in the field of view (usually between 5 and 20 particles) and lag times $0.03\ \text{s} < \tau < 10\ \text{s}$. Fits are performed for lag times $\tau < 2$ s. We estimate the drift from the motion of the center of mass of the particle ensemble, according to the algorithm developed by V. Pelletier and coworkers.[50]

The value of the drag coefficient can be determined from the Einstein relation:

$$D = \frac{k_B T}{f} \quad (5)$$

where k_B is the Boltzmann constant and T the absolute temperature. For a particle of radius R moving in a fluid with viscosity η, the drag coefficient reduces to the Stokes' drag $f = 6\pi\eta R$. Eqn (5) also holds for a particle at a fluid-fluid interface.[11,19] The interfacial drag coefficient depends on the particle three-phase contact angle θ, the radius R, and the viscosities of the two phases and of the interface. The relation between the drag coefficient and the rheology of the interface depends on the material system under study, the assumptions of the hydrodynamic model used for the analysis,[38–40] as well as on the actuation dynamics (e.g. rotation or translation) of the probe.[28]

In this study we present data as the particle drag coefficient f extracted from fits of eqn (3) to the IPM trajectory data. In section 4.1 we will relate f to the rheology of the interface.

3 Results

In this section we present results as follow. We first measure and compare the drag coefficient of particles moving in bulk water with IPM and MSD analysis, thus proving the validity of the method. Then, we study how the polymer influences the position of particles at the water-oil interface and finally we apply IPM to study the adsorption of polymer at the interface for different fluid compositions. For clarity in presenting the results, we will express the polymer concentration in units of 10^{-3} w/w%.

3.1 Drag measurements in water

In an IPM experiment particles are repeatedly brought in contact and then separated by several micrometers ($S \simeq 3-16\ \mu$m) by changing the orientation of the magnetic field (see Fig. 1b). Fig. 2a shows repeated magnetic repulsion curves for the same particle pair, where the particles move in bulk water over a glass surface (so not yet for a system with an oil-water interface). At a separation distance in the order of a particle diameter, particles separate with initial speeds of a few tens of μm/s; at larger separations the velocity decreases due to the lower dipole-dipole force [cf $1/S^4$ in eqn (2)]. We limit the data range for our analysis to $S < 10\ \mu$m, because at higher separations Brownian fluctuations appear in the trajectories. From the fit of every single curve according to eqn (3) we extract an average value for the drag coefficient of $f^{IPM}_{water} = (5.8 \pm 0.6) \cdot 10^{-8}$ Ns/m (weighted average over 15 curves $\pm$ standard error). Plots of S^5 as a function of repulsion time (inset Fig. 2a) show the expected linear relationship for the motion of particles in a Newtonian fluid. Data obtained from attraction curves give similar results as the repulsion curves (data not shown).

Fig. 2b shows an MSD curve obtained from the trajectories of 12 particles undergoing Brownian motion. The red straight line is a fit according to eqn (4). The curve shows the expected linear behavior with slope $\alpha = 1$ as for the motion of a particle in a purely viscous fluid, with an accuracy of 0.2%. From the Stokes-Einstein relation (eqn (5)) we quantify the value of the drag coefficient from 9 measurements to be $f^{MSD}_{water} = (5.9 \pm 0.4) \cdot 10^{-8}$ Ns/m. This value is in agreement with IPM results within the experimental errors, confirming the consistency of the methods.

3.2 Particle position as a function of polymer concentration

Particles bind to the interface only when the polymer is present in the oil phase. Without any polymer, particles do not bind to the interface and sediment to the bottom of the fluid cell. For high polymer concentrations ($c_P > 500 \cdot 10^{-3}$ w/w%) particles transit into the oil phase, which was proven by applying a vertical magnetic force after about 30 minutes and by observing that particles are able to reach the top glass of the fluid cell. For lower concentrations particles remained at the interface. These results

Soft Matter Accepted Manuscript

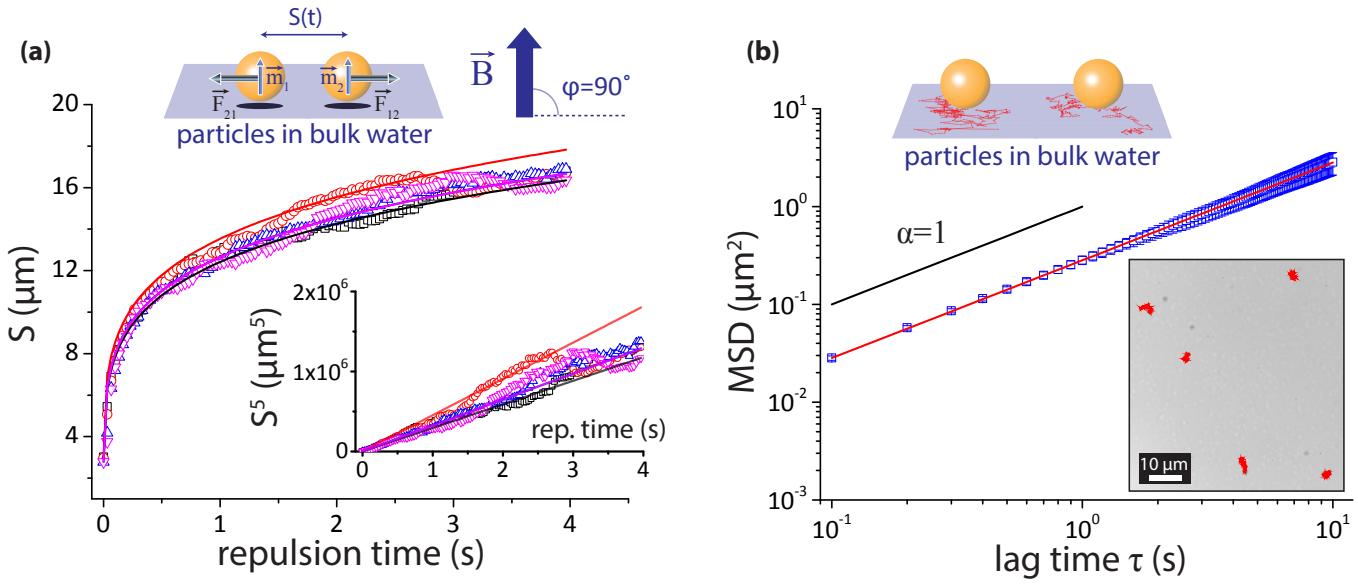

Fig. 2 Particle motion data from Intra-Pair Magnetophoresis (IPM) and Brownian motion experiments, for particles in water near a solid substrate. (a) Center-to-center separation distance S as a function of magnetic repulsion time. Symbols and colours represent experimental data of four repulsion curves for the same pair of magnetic particles, with an average standard deviation between the measured points of about 3%. The solid lines represent fits according to eqn (3). The fitting routine is applied in the range $S < 10\ \mu$m, because at higher separations Brownian fluctuations appear in the trajectories. The inset shows that S^5 scales linearly with repulsion time, in agreement with theory. The variation in slopes is less than 10%. (b) Mean-squared Displacement (MSD) of particle motion extracted from the average of 12 particles; the red line is the fit according to eqn (4) with a standard deviation of 0.2 %. The inset shows an image with particles and superimposed trajectories.

show that it is possible to change particle wettability by varying the polymer concentration in the oil phase, as summarized in Fig. 1d.

3.3 Drag measurement at a water-oil interface

Here, we apply IPM to study the influence of the adsorption of polymer at a water-oil interface as a function of time and fluid composition. We will refer to the range of polymer concentrations as defined in Fig. 1d (low, intermediate, high). In Fig. 3a we show an example of IPM experiments for particles at a water-oil interface. Experiments were recorded at different polymer adsorption times of the interface. At $t_A = 251$ s (black symbols) particles separate tens of μm, with similar distances as compared to the motion of particles in bulk water (Fig. 2a). For longer polymer adsorption times, the inter-particle separation is reduced to a fraction of the particle diameter. The small error bars, represented as the standard deviation of 5 repeated repulsion trajectories, highlight the high reproducibility of IPM trajectories. In Fig. 3b we represent IPM trajectories as S^5 and perform fits according to eqn (3). The data show a linear relationship within the error bars for all times. The linear relationship is observed for all fluid compositions used in this study, proving the linear shear response of the interface to the motion of the probe. If there was a substantial nonlinear contribution to the force, the data would deviate significantly from eqn (3). Interestingly, for long polymer adsorption times and short repulsion times, we observe a very weak non-linearity (Fig. 3b, third panel), which will be discussed in section 4.1.

3.3.1 Low and high polymer concentrations.

Fig. 4 shows measurements of the drag coefficient f as a function of polymer adsorption time for low and high concentrations of polymer and for different ionic strengths of the water phase. Measurements obtained from the same particle pair (points connected by a dashed line in Fig. 4) show time independent values. Variations between values are observed from measurement on different pairs. All measured values are higher than the theoretical Stokes drag coefficient for the particles in their respective bulk fluids, as indicated by the dotted lines in Fig. 4. Results for a low and high polymer concentration yield an average drag coefficient of $f_{low} = (5.1 \pm 0.8) \cdot 10^{-8}$ Ns/m, and $f_{high} = (3.8 \pm 0.6) \cdot 10^{-7}$ Ns/m (for the aqueous phase with 150 mM PBS) respectively.

3.3.2 Intermediate polymer concentrations – high ionic strength.

Data in Fig. 5a show values for f as a function of polymer adsorption time for different initial polymer concentrations and a high salt concentration (150 mM PBS) in the aqueous phase. Data for $c_P = 1 \cdot 10^{-3}$ w/w% show first a constant value for f followed by

This journal is © The Royal Society of Chemistry [year]

Soft Matter Accepted Manuscript

a 100 fold increase over a timespan of a few hours (one time decade). For $c_P = 2 \cdot 10^{-3}$ w/w% the increase is a 1000 fold ($\sim 10^{-7} - 10^{-4}$ Ns/m) within a similar timespan. The time onset for the increase of f shifts towards lower adsorption times for higher initial polymer concentrations, with a similar rate of drag increase. Multiple points measured at a same polymer adsorption time represent data recorded on particle pairs located in the same field of view, with variations of drag coefficients within the experimental errors. Breaks between points, e.g. for $c_P = 1 \cdot 10^{-3}$ w/w% of Fig. 5a, are data recorded on different particle pairs located at different positions in the water-oil interface, showing a similar interface ageing. Drag coefficients extracted from magnetic attractions and repulsions trajectories show no significant differences (ESI†, S2).

3.3.3 Intermediate polymer concentrations – low ionic strength.

Data (Fig. 5b) for a low salt concentration (20 mM PBS) in the aqueous phase shows for all concentrations first a constant value of f followed by a time dependent increase. When comparing these results with the one obtained for a high ionic strength solution (Fig. 5a) we observe that the time onset for the drag coefficient increase occurs at higher adsorption times and within a narrower timespan. Moreover, the rate of increase for f strongly depends on the initial polymer concentration. In particular, for $c_P = 1 \cdot 10^{-3}$ w/w% f increases of a factor of 2 in a time span of one decade, which is significantly lower than the 100 fold increase observed for the high ionic strength solution and same polymer concentration (Fig. 5a). For c_P equal to 3 and $4 \cdot 10^{-3}$ w/w%, we observe a similar 1000 fold increase. The variability between particle pairs is within the experimental errors.

4 Discussion

4.1 Rheometry by Intra-Pair Magnetophoresis

In an IPM experiment, pairs of micrometer-sized magnetic particles are repeatedly attracted and repelled by well-controlled magnetic dipole-dipole forces. From the forces (∼pN), displacements ($\sim \mu$m) and velocities ($\sim \mu$m/s) of the particles we are able to quantify the interfacial viscous drag within a few seconds (~ 5 s) and over long timescales (several hours), making this technique suitable to study time dependent phenomena such as the early stages of adsorption of macromolecules at a fluid-fluid interface as well as the aging of interfacial systems.

The size of the probe sets the sensitivity of the system to interfacial viscosities as low as $\eta_s = 7 \cdot 10^{-9}$ Ns/m [using $\eta_{water} = 1$ mPa·s, $\eta_{oil} = 6$ mPa·s, and $a \simeq 1$ μm, see eqn (1)], while the upper limit is determined mainly by the tracking accuracy of particles. For example, if we consider a magnetic field of 50 mT, a measurement time of 30 s and a particle displacement of 1 μm, we can measure a drag coefficient $f \sim 10^{-3}$ Ns/m, which corresponds to interfacial viscosities in the order of $\eta_S \sim 10^{-3}$ Ns/m (for $\theta = 90°$).[39] Our measurements show a dynamic range of about 4 orders of magnitude (Fig. 5), which is comparable to other active methods based on optical[35–37] and magnetic tweezers[23–28] experiments. An important advantage of IPM is that commercially available magnetic particles are used and that data can be acquired with high statistics by tracking many particle pairs simultaneously.

The accuracy of the drag coefficient determined by IPM is mainly determined by the uncertainty of the magnetic moment m of particles, which was measured to be about 8 % for the M-270 particles used in this study.[41] The hydrodynamic coupling between the particles[51] introduces a systematic error, which scales as $\sim 1/S$. Reenen et al.[41] performed numerical simulations of intra-pair motion on the very same particles of this study, showing that the hydrodynamic coupling leads to an underestimation of m of about 0.8 %. Here, for our experiments we consider a total uncertainty of magnetization of 10 %. The standard error from repeated measurement on the same pair (as shown in Fig. 2a) is less than 10 %, showing a good reproducibility of the method.

Superparamagnetic particles are know to have a small remanent magnetic moment.[52,53] A change of the orientation of the magnetic field would exert a mechanical torque, which may introduce capillary dipolar interactions for particles at the water-oil interface.[54] The maximum magnetic torque $\vec{\tau} = \vec{m} \times \vec{B}$ applicable on the particles of this study has been calculated by van Reenen et al.[53] to be $4 \cdot 10^{-18}$ Nm/rad (for a magnetic field of 36 mT). Xie et al.[55] performed lattice Boltzmann simulations of capillary deformations for magnetic Janus particles at a fluid-fluid interface. In the limit of small interfacial deformation, the required torque to induce capillary deformation is $\sim 10^{-13}$ Nm/rad, which is much larger than the magnetic torque. This proves that magnetically induced deformation of the interface are negligible.

IPM trajectories obtained for particles moving in water over a surface (Fig. 2a) are correctly described by eqn (3), which holds for a system with linear viscous behavior. The corresponding drag coefficient is about a factor of 2 higher than the theoretical Stokes drag $f^{th}_{water} = 2.6 \cdot 10^{-8}$ Ns/m for a particle in bulk water. We attribute the higher value to wall effects, as the effective viscosity increases when the distance to the surface becomes comparable to the particle radius.[56] According to the model by Leach et al.,[57] the correction factor for a particle translating over and touching a surface is 1.77. Data of f obtained from Brownian motion experiments give comparable results, proving the validity of IPM method to quantify the shear viscosity of fluids.

For further comparison, we recorded the drag coefficient at a water-oil interface using both IPM and MSD analysis. The resulting values of f are comparable only for a low polymer concentration and for short adsorption times (ESI†, Fig. S4). For higher concentrations and longer adsorption times we measure systematically lower values from the MSD analysis. We attribute

Soft Matter Accepted Manuscript

this discrepancy to an incorrect drift correction in MSD (ESI†, Fig. S3d). With the number of particles in the MSD measurement (4 to 20), a sufficient drift correction could not be achieved in the case of high interfacial viscosity. This is in agreement with the results showed by Samaniuk et al.,[19] where the authors demonstrated that for high interfacial viscosities (e.g. $\eta_S > 10^{-6}$ Ns/m) the diffusivity of particles becomes comparable to the static noise of the system, whose incorrect estimation leads to an apparent lower viscosity.

In active microrheology the geometry, the size of the probe (Boussinesq number) and the dynamics of the actuation (e.g. rotation and translation) play an important role. The deformation flow field of the interface potentially mixes different dynamic modes (e.g. shear and dilatation), thereby complicating the interpretation of the data into meaningful rheological quantities. This complication arises also from the lack of an analytical solution for the steady motion of a sphere in an ideal 2D fluid (Stokes' paradox), so one must rely on numerical solutions. Danov et al.[38] modeled a fluid-fluid interface as a compressible 2D-fluid and solved numerically the Navier-Stokes equation to obtain the values of the drag coefficient f as a function of the particle contact angle, the dilatational and the shear viscosity of the interface. On the other hand, Fischer et al.[39] assumed that Marangoni forces were instantly compensated by the fast diffusion of macromolecules at the interface (e.g. surfactants), so that the interface behaves as 2D-incompressible. Therefore, care must be taken when interpreting experiments of translating probes at an interface, as an incompressibility of the dilute layer ($Bo << 1$) could contribute to the particle's drag increase, even for completely inviscid layers. This was studied by Zell et al.[28] using rotating magnetic micro-buttons to induce only surface shear to surfactant monolayers at an air-water interface. The authors demonstrated that the surfactants had no measurable surface shear viscosity, in contrast to results from translational studies.

From IPM experiments performed at the water-oil interface in the presence of polymer, we show that the response of the interface to the motion of the probe is essentially linear (Fig. 3), as expected for a purely viscous system as described by eqn (3). The observed increase of drag as a function of polymer adsorption time (Fig. 5) could in principle be caused by an increase of interfacial viscosity or interfacial incompressibility, as proposed by Fischer et al..[39] The polymer studied in our paper is a synthetic silicone polymer with random side chains, having in solution a 15 nm radius of gyration. When the polymer adsorbs at the interface, we expect polymer entanglement and reptation to play a role,[18,58] which should generate dissipative effects upon actuation of a particle at the interface. Therefore, we attribute the polymer-dependent increase of drag coefficient to an increase of interfacial viscosity. However, we cannot exclude that also incompressibility effects plays a role. This could be further investigated by comparing experiments of particle translation with particle rotation,[53] where only shear deformations are introduced at the interface.[28]

Interestingly, for long polymer adsorption times we observed a very weak non-linearity at short separation distances (Fig. 3b). This may point to a non-linear response of the aged interface that depends on particle velocity or magnitude of the applied magnetic force, which could correspond to an increase of the elastic response or a shear thickening of the interface. We have analysed the non-linearity by a history dependent viscosity[48,49] or by modelling the interface as a power-law fluid.[23] However, it appeared that the non-linearity is too small to be able to extract meaningful non-Newtonian parameters from our experiment.

An interesting feature of IPM experiments is that data is generated in two different pair actuation modes, namely repulsion and attraction. In our measurements we did not observed any significant difference between drag values obtained by magnetic repulsion and magnetic attraction (section S2 ESI†). Nonetheless, in a system with strong nonlinear effects, IPM may be used to compare the two perturbation modes of the interface, with emphasis on elongation in the case of particle separation, and compression in the case of particle attraction.

4.2 Particle position as a function of polymer concentration

In section 3.1 we observed that the position of particles with respect to the water-oil interface is modulated by the amount of polymer present in the oil phase. We interpret this change in particle wettability as an interplay between interfacial forces and electrostatic interaction between particles and polymers. The surface of the magnetic particles is functionalized with carboxylic groups and becomes negatively charged when immersed in a solution with a pH above the isoelectric point of the particles (pI = 4.5).[59] Dynamic surface tension measurements (data not shown) have shown that the surface tension decreases as a function of time and polymer concentrations, showing that the polymers adsorb at the interface also in the absence of magnetic particles. The very low solubility of the polymer in water causes only the amine groups to penetrate the interface into the water phase. There the polymer becomes positively charged, giving the possibility to interact electrostatically with the negatively charged magnetic particles[5,60]. This electrostatic attraction is counterbalanced by interfacial forces that keep the particles at the fluid-fluid interface. Only at high concentrations of polymer the particles are able to transit into the oil phase. A similar result was obtained by Binks et al.,[61] who demonstrated that the wettability of silica nanoparticles can be tuned by changing the amount of cationic surfactant adsorbed on the surface of the nanoparticles, leading to a double inversion Pickering emulsion.

Measurements at low polymer concentrations (e.g. $c_P = 0.5 \cdot 10^{-3}$ w/w%) show values of f close to a particle diffusing in bulk

Soft Matter Accepted Manuscript

This journal is © The Royal Society of Chemistry [year]

water (Fig. 4). Here, we estimate the interfacial polymer concentration to be low (ESI†, S4) and we expect a weak interaction between the particles and the interface. During experiments we observed the detachment of particles from the interface. This can be explained only with a small value of the contact angle θ. The trapping energy of a particle at the interface is determined by the contributions of the surface free energies of the three phases (particle surface, water, oil) and can be calculated with the relation $\Delta E = -\pi R^2 \gamma \cdot (1 - |\cos\theta|)^2$,[62] where γ is the surface tension. A typical value for the maximum trapping energy is $\Delta E \simeq 4.5 \cdot 10^7$ k_B T (using $\gamma = 3 \cdot 10^{-2}$ N/m, $\theta = 90°$), making the desorption process very unlikely. The electrostatic interaction between the polymer and the particle surface modulates the particle-oil surface free energy, i.e. the particle contact angle, and $\Delta E \approx k_B T$ only for $\theta < 1°$. At this low polymer concentration the interfacial viscosity η_S can be expected to be low and the drag coefficient of the particle is dominated by the sub-phase viscosity ($Bo << 1$). In this regime, it is difficult to extract reliable interfacial viscosities, as changes of the particle contact angle would contribute to an apparent change in the interfacial viscosity, even for an inviscid interface.[28]

For a high polymer concentration in the oil phase ($c_P = 500 \cdot 10^{-3}$ w/w%), the particles at the interface become densely coated with polymer and thereby become hydrophobic, which allows them to transit into the oil phase as confirmed by the drag measurements (Fig. 4). Values for f are a factor of two higher than the Stokes drag for a particle in the neat bulk oil ($f^{th}_{oil} = 1.6 \cdot 10^{-7}$ Ns/m). This difference can be explained in a similar way as for the transport of a particle close to a surface, where the vicinity of the particle to the fluid interface has the effect of increasing the effective viscosity.[63] Moreover, the presence of polymer might increase the bulk oil viscosity. The measured drag coefficient shows a higher variability compared to measurements of particles trapped at the interface (lower polymer concentration); this may reflect variations in how a particle transits into the oil phase. We rule out that the particle crossing is the result of lowering the water-oil surface tension, as previously observed by Tsai and coworkers.[64] For a high concentration of polymer the surface tension decreases only by about a factor of 3 with respect to a pristine water-oil interface. This change would not be sufficient for the particles to cross the interface, even in the presence of a high magnetic force. For example, a force of 100 pN would result in a vertical displacement of an adsorbed particle by about 5 nm. Only for an ultra-low surface tension ($\approx 10^{-6}$ N/m) the interface crossing would be possible.[64] In summary, the drag measurements of Fig. 4 confirm the qualitative results found in section 3.2: for low concentrations particles are weakly bound to the interface and are more immersed in the water phase; for high concentrations particles can cross the interface and move into the oil phase.

For intermediate polymer concentrations we observe variations of interfacial drag coefficients over several orders of magnitude (Fig. 5). The drag coefficient of particles trapped at a fluid-fluid interface is influenced by the particle contact angle, which is unknown in our experiments. Aaron et al.[65] compared theoretical models and experiments of particle drag coefficients at a fluid-fluid interface. For a water-air interface with a viscosity ratio $\eta_{water}/\eta_{air} \simeq 10^3$, a change of the particle contact angle between 0° and 90° gives a decrease of the particle drag coefficient of about 65%. In the case of nanoparticles at a water-alkane interface, Wang et al.[66] showed that the drag coefficient increase for increasing viscosity of the alkanes, with an increase of about 60% for $\eta_{C16}/\eta_{water} \simeq 3.5$. In our system the viscosity ratio is $\eta_{oil}/\eta_{water} \simeq 6$, so we expect that a change of contact angle would give only a small change of drag. Therefore, the variation over several orders of magnitude that we observe for the interfacial drag coefficients, is dominated by changes of interfacial viscosity ($Bo >> 1$) rather than changes of the particle contact angle. The high sensitivity to interfacial viscosity is in agreement with the large value of the Boussinesq number in our system (eqn (1)).

4.3 Adsorption of polymers to the interface

The adsorption of macromolecules to a fluid-fluid interface involves a two-step process: diffusive transport from the bulk fluid of one of the two phases to the proximity of the interface, and thereafter a molecular adsorption process that may be influenced by an energy barrier, such as an electrostatic barrier for charged species, or a steric barrier due to the presence of already adsorbed molecules.[8,9] At short times, $t \to 0$, polymers adsorb to a pristine interface without steric hindrance. In absence of an energy barrier for adsorption, the surface coverage Γ (mol/m^2) can be estimated using the Ward-Tordai equation:[67]

$$\Gamma(t) = 2 c_P \sqrt{\frac{Dt}{\pi}} \qquad (6$$

For concentrations below the overlap concentration c^*,[68] the diffusion constant D can be estimated by assuming the polymer to be a sphere of radius R_G (see section 2.1). The results in Fig. 4 for low c_P and short adsorption times indicate that the interface is in the dilute regime[69] and that the amount of polymer is not sufficient to change the mobility of the particles (ESI†, S4). Graham et al.[10] showed that for protein adsorbing to a water-air interface eqn (6) is valid for a relative surface coverage of $\Gamma_R < 10\%$. A similar conclusion has been reported for the early stages of adsorption of polymers at a water-air interface[9] and for polymer-functionalized nanoparticles at a water-n-Decane interface measured with pendant-drop tensiometry.[13]

At long times the adsorption rate is lowered due to the presence of only few remaining adsorption sites in the interfacial monolayer and eqn (6) is not valid anymore. Here, the interactions between the adsorbed polymers (e.g. hydrogen bonding, hydropho-

Soft Matter Accepted Manuscript

bic or electrostatic interactions) can contribute to an increase of the interfacial viscosity.[2] This is shown in our experiments for intermediate polymer concentrations (Fig. 5a), where the drag coefficient of particles at the interface increases over several orders of magnitude in a timespan of a few hours. The time onset for drag increase shifts towards shorter adsorption times for increasing initial polymer concentration in the oil phase, which is consistent with a higher diffusive flux of polymer to the interface (ESI†, S4). Data recorded on different particle pairs within the same field of view show variabilities within the experimental error. Data recorded on particle pairs located at different positions of the water-oil interface show a similar increasing rate of drag, suggesting a homogeneous interface ageing. Moreover, this increase is similar for all concentrations, following a power-law relationship. A similar behavior was observed by Maestro et al.,[18] where they studied the interfacial viscosity of poly(*tert*-butyl-acrylate) of different molecular weights at a water-air interface using passive microrheology. They showed that the interfacial viscosity follows a power-law increase as a function of surface concentration ($\eta_s \sim \Gamma^{\beta}$), with increasing values of β for polymers with a higher molecular weight. This reasoning cannot be directly applied to our data, as measurements were not performed at equilibrium. Nonetheless, under certain assumptions (ESI†, S5) we estimate an exponent that suggests a strong polymer-polymer interaction at the interface. This is also confirmed by the observed increase of drag coefficient over several orders of magnitude in a short time span.

The kinetics of polymer adsorption and interface ageing are influenced by the ionic strength of the water phase, as shown in Fig. 5b. A low ionic strength in the aqueous phase may enhance the electrostatic interaction of the polymers at the fluid-fluid interface due to unscreened charges of the amine groups exposed to the water phase.[5] The enhanced electrostatic interaction may favor a stretched conformation of the polymer at the interface, increasing repulsion between polymer chains, and thereby lowering the probability for further polymer adsorption.[70] This is suggested by a significantly lower increase of drag coefficient for $c_P = 1 \cdot 10^{-3}$ w/w% as compared to a high salt concentration (Fig 5a). Moreover, the time onset for the increase of the drag coefficient for c_P equal to 2, 3 and $4 \cdot 10^{-3}$ w/w% is shifted towards longer adsorption times, indicating slower adsorption kinetics. The increase of drag coefficients spans a similar dynamic range as compared to a high ionic strength solution, with a similar rate of increase. The dependency on the initial polymer concentration suggests a non-equilibrium interface ageing, where the evolution of the interface is determined by the early stages of polymer adsorption.[71]

5 Conclusions

We have presented an interfacial rheometry technique wherein pairs of micrometer-sized magnetic particles are repeatedly attracted and repelled by well-controlled magnetic dipole-dipole interactions, so-called interfacial rheometry by Intra-Pair Magnetophoresis. We have validated the technique first by measuring particle drag coefficients in bulk water and by comparing the results to Brownian motion analysis, showing a good agreement between both methods. Thereafter we applied IPM to quantify interfacial drag in a materials system with adsorption of an amino-modified polymer to a water-oil interface. In absence of polymer in the oil phase, the particles stay in the water phase and do not attach to the fluid-fluid interface. For high polymer concentrations, the particles transit into the oil phase due to polymer binding to the particles by electrostatic interactions. For intermediate polymer concentration, the particles remain in the fluid-fluid interface and experience a drag that depends strongly on polymer concentration, on time, and on the ionic strength of the aqueous phase. Measurements as a function of polymer adsorption time show an increase of interfacial drag by more than three orders of magnitude over a timespan of a few hours, suggesting a strong polymer-polymer interaction at the interface.

The IPM experiments show that the hydrodynamic response of the interface in the presence of adsorbed polymer is essentially Newtonian. Interestingly, a very small deviation appeared for long polymer adsorption times and small particle separations, which may point to a weak nonlinear response of the interface. In our experiment large displacement amplitudes were used, which might influence elastic structures in the system.[25] To study the viscoelastic response at weak perturbation, the IPM technique may be applied with small amplitudes, e.g. by imposing onto the particles an oscillatory motion with amplitudes of only tens of nanometers and frequencies of tens of Hz. For further study, it may be interesting to look at possible differences between separation and attraction, where differences due to interface elongation and compression may be revealed. Also it would be interesting to apply IPM to other materials systems, such as albumin[26] or lysozyme[23] at an air-water interface, or particle laden fluid interfaces.[11] Finally, the application of higher magnetic forces (e.g. with stronger magnetic fields or particles with a higher magnetic content) may more deeply reveal non-linear responses of the interface.

The sensitivity of the IPM method, the short time required for recording a single measurement point, the relatively simple instrumentation that is needed, the possibility to follow simultaneously many particles over a long period of time, and the fact that commercially available particles can be used as probes, make IPM a very versatile method to study interfacial viscosity in a wide variety of soft-matter materials applications.

Acknowledgements

The authors thank Nicolas Bremond and Perrine Colliat-Dangus from the Institute of Chemistry, Biology and Innovation at ESPCI

Soft Matter Accepted Manuscript

This journal is © The Royal Society of Chemistry [year]

Paris for stimulating discussions. The research leading to these results has received funding from the European Commission's Seventh Framework Programme (FP7/2007-2013) under the grant agreement BIOMAX (project n° 264737).

References

1 B. S. Murray and E. Dickinson, *Food Science and Technology International, Tokyo*, 1996, **2**, 131–145.

2 M. A. Bos and T. van Vliet, *Advances in Colloid and Interface Science*, 2001, **91**, 437–471.

3 A. Ammala, *International Journal of Cosmetic Science*, 2013, **35**, 113–124.

4 G. Kaufman, R. Boltyanskiy, S. Nejati, A. R. Thiam, M. Loewenberg, E. R. Dufresne and C. O. Osuji, *Lab on a Chip*, 2014, **14**, 3494.

5 G. Kaufman, S. Nejati, R. Sarfati, R. Boltyanskiy, M. Loewenberg, E. R. Dufresne and C. O. Osuji, *Soft Matter*, 2015, **11**, 7478–7482.

6 S. Kinge, M. Crego-Calama and D. N. Reinhoudt, *ChemPhysChem*, 2008, **9**, 20–42.

7 L. Isa, K. Kumar, M. Müller, J. Grolig, M. Textor and E. Reimhult, *ACS Nano*, 2010, **4**, 5665–5670.

8 J. Eastoe and J. Dalton, *Advances in Colloid and Interface Science*, 2000, **85**, 103–144.

9 V. P. Gilcreest, K. A. Dawson and A. V. Gorelov, *Journal of Physical Chemistry B*, 2006, **110**, 21903–21910.

10 D. Graham and M. Phillips, *Journal of Colloid and Interface Science*, 1979, **70**, 403–414.

11 A. J. Mendoza, E. Guzmán, F. Martínez-Pedrero, H. Ritacco, R. G. Rubio, F. Ortega, V. M. Starov and R. Miller, *Advances in Colloid and Interface Science*, 2014, **206**, 303–319.

12 C. Monteux, *Comptes Rendus Physique*, 2014, **15**, 775–785.

13 A. Nelson, D. Wang, K. Koynov and L. Isa, *Soft Matter*, 2015, **11**, 118–129.

14 F. Ortega, H. Ritacco and R. G. Rubio, *Current Opinion in Colloid & Interface Science*, 2010, **15**, 237–245.

15 O. S. Deshmukh, D. van den Ende, M. C. Stuart, F. Mugele and M. H. Duits, *Advances in Colloid and Interface Science*, 2015, **222**, 215–227.

16 P. Cicuta and A. M. Donald, *Soft Matter*, 2007, **3**, 1449.

17 G. G. Fuller and J. Vermant, *Annual Review of Chemical and Biomolecular Engineering*, 2012, **3**, 519–543.

18 A. Maestro, L. J. Bonales, H. Ritacco, T. M. Fischer, R. G. Rubio and F. Ortega, *Soft Matter*, 2011, **7**, 7761.

19 J. R. Samaniuk and J. Vermant, *Soft Matter*, 2014, **10**, 7023–7033.

20 M. H. Lee, S. P. Cardinali, D. H. Reich, K. J. Stebe and R. L. Leheny, *Soft Matter*, 2011, **7**, 7635.

21 T. M. Squires and J. F. Brady, *Physics of Fluids*, 2005, **17**, 073101.

22 A. M. Puertas and T. Voigtmann, *Journal of Physics: Condensed Matter*, 2014, **26**, 243101.

23 D. B. Allan, D. M. Firester, V. P. Allard, D. H. Reich, K. J. Stebe and R. L. Leheny, *Soft Matter*, 2014, **10**, 7051–7060.

24 A. Brasovs, J. Cīmurs, K. Ērglis, A. Zeltins, J.-F. Berret and A. Cēbers, *Soft Matter*, 2015, **11**, 2563–2569.

25 S. Choi, S. Steltenkamp, J. Zasadzinski and T. Squires, *Nature Communications*, 2011, **2**, 312.

26 P. Dhar, Y. Cao, T. M. Fischer and J. a. Zasadzinski, *Physical Review Letters*, 2010, **104**, 016001.

27 M. H. Lee, D. H. Reich, K. J. Stebe and R. L. Leheny, *Langmuir*, 2010, **26**, 2650–2658.

28 Z. A. Zell, A. Nowbahar, V. Mansard, L. G. Leal, S. S. Deshmukh, J. M. Mecca, C. J. Tucker and T. M. Squires, *Proceedings of the National Academy of Sciences*, 2014, **111**, 3677–3682.

29 V. Prasad, S. A. Koehler and E. R. Weeks, *Physical Review Letters*, 2006, **97**, 176001.

30 G. Pesce, A. C. De Luca, G. Rusciano, P. A. Netti, S. Fusco and A. Sasso, *Journal of Optics A: Pure and Applied Optics*, 2009, **11**, 034016.

31 A. Yao, M. Tassieri, M. Padgett and J. Cooper, *Lab on a Chip*, 2009, **9**, 2568.

32 L. G. Wilson and W. C. K. Poon, *Physical Chemistry Chemical Physics*, 2011, **13**, 10617.

33 M. Tassieri, F. D. Giudice, E. J. Robertson, N. Jain, B. Fries, R. Wilson, A. Glidle, F. Greco, P. A. Netti, P. L. Maffettone, T. Bicanic and J. M. Cooper, *Scientific Reports*, 2015, **5**, 8831.

34 D. Mizuno, D. A. Head, F. C. MacKintosh and C. F. Schmidt, *Macromolecules*, 2008, **41**, 7194–7202.

35 C. Y. Park, H. D. Ou-Yang and M. W. Kim, *Review of Scientific Instruments*, 2011, **82**, 094702.

36 R. Shlomovitz, A. A. Evans, T. Boatwright, M. Dennin and A. J. Levine, *Physical Review Letters*, 2013, **110**, 137802.

37 C. Y. Park and M. W. Kim, *The Journal of Physical Chemistry B*, 2015, **119**, 5315–5320.

38 K. Danov, R. Aust, F. Durst and U. Lange, *Journal of Colloid and Interface Science*, 1995, **175**, 36–45.

39 T. M. Fischer, P. Dhar and P. Heinig, *Journal of Fluid Mechanics*, 2006, **558**, 451.

40 T. M. Squires and T. G. Mason, *Annual Review of Fluid Mechanics*, 2010, **42**, 413–438.

41 A. van Reenen, Y. Gao, A. H. Bos, A. M. de Jong, M. A. Hulsen, J. M. J. den Toonder and M. W. J. Prins, *Applied Physics Letters*, 2013, **103**, 043704.

42 A. van Reenen, A. M. de Jong, J. M. J. den Toonder and M. W. J. Prins, *Lab on a Chip*, 2014, **14**, 1966.

43 A. S. Sergeeva, D. A. Gorin and D. V. Volodkin, *Bio-*

Soft Matter Accepted Manuscript

NanoScience, 2014, **4**, 1–14.
44 S. Je Lee and M. Rosenberg, *LWT - Food Science and Technology*, 2000, **33**, 80–88.
45 M. Irmscher, A. M. de Jong, H. Kress and M. W. Prins, *Biophysical Journal*, 2012, **102**, 698–708.
46 J. C. Crocker and D. G. Grier, *Journal of Colloid and Interface Science*, 1996, **179**, 298–310.
47 D. Blair and E. R. Dufresne, *http://site.physics.georgetown.edu/matlab/index.html*.
48 T. G. Mason and D. A. Weitz, *Physical Review Letters*, 1995, **74**, 1250–1253.
49 J. van der Gucht, N. a. M. Besseling, W. Knoben, L. Bouteiller and M. a. Cohen Stuart, *Physical Review E*, 2003, **67**, 051106.
50 V. Pelletier, N. Gal, P. Fournier and M. L. Kilfoil, *Physical Review Letters*, 2009, **102**, 188303.
51 J. Liu, M. L. Gardel, K. Kroy, E. Frey, B. D. Hoffman, J. C. Crocker, A. R. Bausch and D. A. Weitz, *Physical Review Letters*, 2006, **96**, 118104.
52 X. J. Janssen, A. J. Schellekens, K. van Ommering, L. J. van IJzendoorn and M. W. J. Prins, *Biosensors and Bioelectronics*, 2009, **24**, 1937–1941.
53 A. van Reenen, F. Gutiérrez-Mejía, L. J. van IJzendoorn and M. W. J. Prins, *Biophysical Journal*, 2013, **104**, 1073–1080.
54 P. A. Kralchevsky and K. Nagayama, *Advances in Colloid and Interface Science*, 2000, **85**, 145–192.
55 Q. Xie, G. B. Davies, F. Günther and J. Harting, *Soft Matter*, 2015, **11**, 3581–3588.
56 H. Brenner, *Chemical Engineering Science*, 1961, **16**, 242–251.
57 J. Leach, H. Mushfique, S. Keen, R. Di Leonardo, G. Ruocco, J. M. Cooper and M. J. Padgett, *Physical Review E*, 2009, **79**, 026301.
58 A. Maestro, H. M. Hilles, F. Ortega, R. G. Rubio, D. Langevin and F. Monroy, *Soft Matter*, 2010, **6**, 4407.
59 N. Wise, T. Grob, K. Morten, I. Thompson and S. Sheard, *Journal of Magnetism and Magnetic Materials*, 2015, **384**, 328–334.
60 B. A. Noskov, *Current Opinion in Colloid & Interface Science*, 2010, **15**, 229–236.
61 B. P. Binks, L. Isa and A. T. Tyowua, *Langmuir*, 2013, **29**, 4923–4927.
62 P. Pieranski, *Physical Review Letters*, 1980, **45**, 569–572.
63 E. Bart, *Chemical Engineering Science*, 1968, **23**, 193–210.
64 S. S. H. Tsai, J. S. Wexler, J. Wan and H. A. Stone, *Lab Chip*, 2013, **13**, 119–125.
65 A. Dörr and S. Hardt, *arXiv:1502.05488*, 2015, 1–11.
66 D. Wang, S. Yordanov, H. M. Paroor, A. Mukhopadhyay, C. Y. Li, H.-J. Butt and K. Koynov, *Small*, 2011, **7**, 3502–3507.
67 A. F. H. Ward and L. Tordai, *The Journal of Chemical Physics*, 1946, **14**, 453.
68 R. A. L. Jones and R. W. Richards, *Polymers at Surfaces and Interfaces*, Cambridge University Press, Cambridge, 1984.
69 F. Monroy, L. R. Arriaga and D. Langevin, *Physical Chemistry Chemical Physics*, 2012, **14**, 14450.
70 D. Langevin, *Advances in Colloid and Interface Science*, 2014, **207**, 121–130.
71 P. de Gennes, *Advances in Colloid and Interface Science*, 1987, **27**, 189–209.

Soft Matter Accepted Manuscript

This journal is © The Royal Society of Chemistry [year]

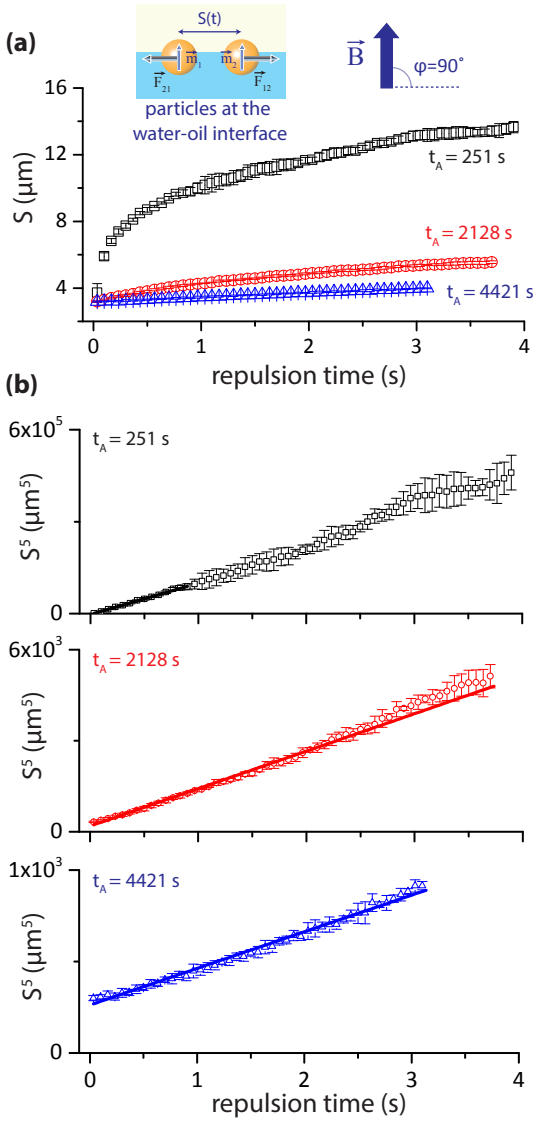

Fig. 3 Particle motion data from Intra-Pair Magnetophoresis (IPM) experiments, for particles at a water-oil interface. Experiments were performed for an aqueous solution with 150 mM PBS and a polymer concentration in the oil phase of $c_P = 2 \cdot 10^{-3}$ w/w%. (a) Center-to-center separation distance S as a function of magnetic repulsion time. Every curve is extracted from the average of 5 consecutive repulsion trajectories, with standard deviations as error bars. Every colour represents experiments recorded at different polymer adsorption times (t_A) of the interface. (b) Particle trajectories as S^5 (symbols) with fits (solid lines) according to eqn (3). The fitting routine is applied in the range $S < 10$ μm, because at higher separations Brownian fluctuations appear in the trajectories. All the curves are shown at a half of the sampling rate of the experiments (30 fps) for clarity.

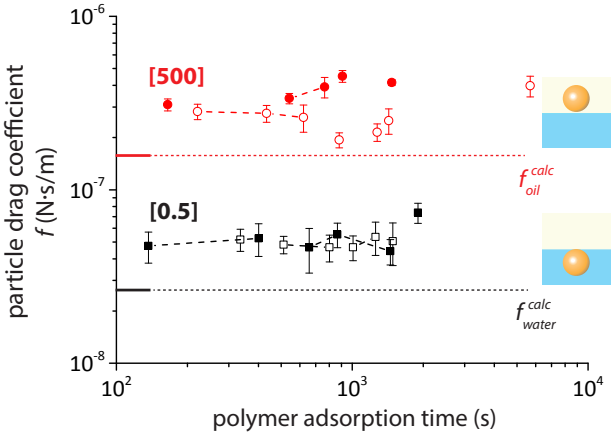

Fig. 4 Particle interfacial drag coefficient f as a function of adsorption time of polymer at the oil-water interface, extracted from IPM analysis for low polymer concentration [c_P] (black squares) and for high polymer concentration (red circles). The polymer concentration is expressed in units 10^{-3} w/w%. The aqueous solution contains 15 mM PBS (open symbols) or 150 mM PBS (solid symbols). The dotted lines represent the calculated Stokes drag of a particle in bulk water (black) or in bulk oil (red). For a low polymer concentration, the particles are attached to the interface but are situated mainly on the water side. For a high polymer concentration, particles transit to the oil side of the interface. Every measurement point is extracted from a fit according to eqn (3) for the average of 5 curves recorded on the same particle pair. Measurement points connected by a dashed line (guide to the eye) are recorded on the same particle pair. Error bars include fitting errors and a variation due to an uncertainty of magnetic susceptibility of 10 %.

Soft Matter Accepted Manuscript

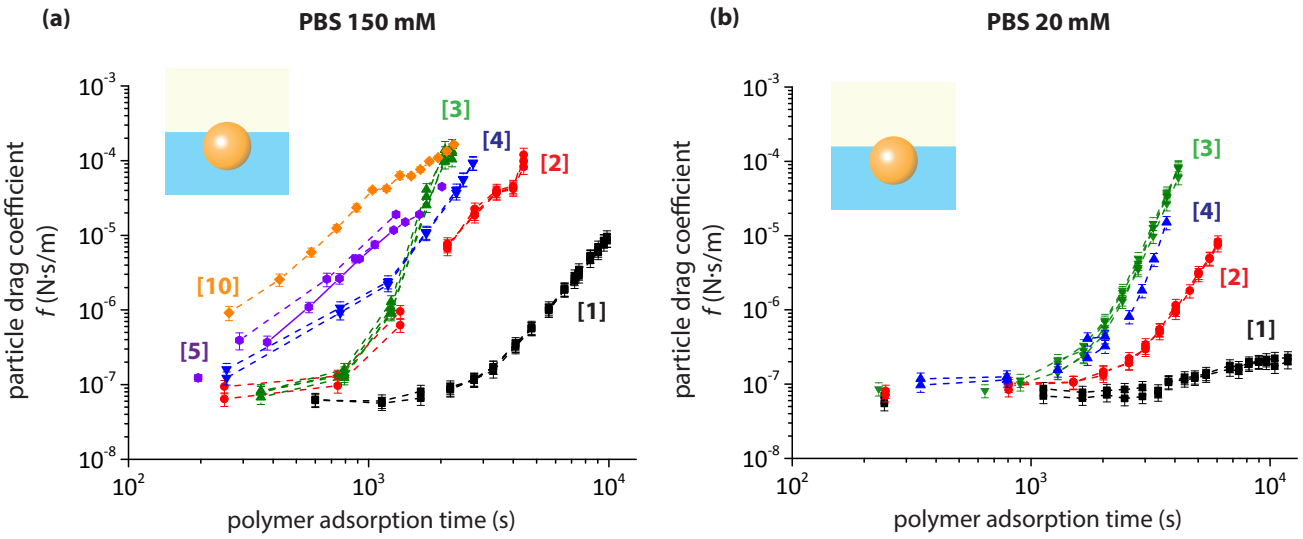

Fig. 5 Particle interfacial drag coefficient f as a function of polymer adsorption time (t_A) for intermediate polymer concentrations [c_P] expressed in units 10^{-3} w/w%. Panel (a) shows data for 150 mM PBS and panel (b) for 20 mM PBS. Every measurement point is extracted from a fit according to eqn (3) for the average of 5 curves of the same particle pair. Error bars include fitting errors and an uncertainty in the magnetic susceptibility of the particles of 10 %. Points connected by a dashed line (guide to the eye) are recorded on the same particle pair. Multiple points at a same polymer adsorption time represent data recorded on particle pairs in the same field of view, with a variability within the experimental errors.

Soft Matter Accepted Manuscript

This journal is © The Royal Society of Chemistry [year]

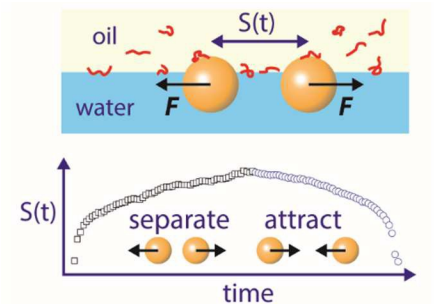

Pairs of magnetic particles at an oil-water interface are repeatedly separated and attracted to quantify the polymer-dependent interfacial drag.

Soft Matter Accepted Manuscript